Title
Plasmon-induced enhancement of intra-ensemble FRET in quantum dots on wrinkled thin films

Journal
Optical Materials Express, 3(3)

ISSN
2159-3930

Authors
Ferri, C. G. L
Inman, R. H
Rich, B.
et al.

Publication Date
2013-02-06

DOI
10.1364/OME.3.000383

Plasmon-induced enhancement of intra-ensemble FRET in quantum dots on wrinkled thin films

C. G. L. Ferri,[1] R. H. Inman,[2] B. Rich,[2] A. Gopinathan,[1] M. Khine,[3] and S. Ghosh[1,*]

[1]*School of Natural Sciences, University of California, 5200 N. Lake Rd., Merced, CA 95343, USA*
[2]*School of Engineering, University of California, 5200 N. Lake Rd., Merced, CA 95343, USA*
[3]*Department of Bioengineering, University of California, Irvine, CA 92697, USA*
**sghosh@ucmerced.edu*

Abstract: We demonstrate increased intra-ensemble energy transfer (ET) in monodispersed semiconducting quantum dots (QDs), mediated by localized plasmons on metallic thin films with nano-scale wrinkles. The increased ET results in a net spectral red-shift, up to three-fold increase in emission intensity, and a faster radiative recombination rate of the ensemble. The extent of the red-shift is dependent on QD size, and is largest for the QDs where the absorption spectrum overlaps the plasmonic resonance of the film. This effect has a uniform, macroscopic manifestation and may provide an inexpensive option of improving performance of QD based photovoltaic devices.

OCIS codes: (250.5403) Plasmonics; (250.5230) Photoluminescence; (310.6628) Subwavelength structures, nanostructures.

References and links

1. J. R. Lakowicz, "Radiative decay engineering: biophysical and biomedical applications," Anal. Biochem. **298**(1), 1–24 (2001).
2. K. T. Shimizu, W. K. Woo, B. R. Fisher, H. J. Eisler, and M. G. Bawendi, "Surface-enhanced emission from single semiconductor nanocrystals," Phys. Rev. Lett. **89**(11), 117401 (2002).
3. D. K. Gramotnev and S. I. Bozhevolnyi, "Plasmonics beyond the diffraction limit," Nat. Photonics **4**(2), 83–91 (2010).
4. F.-J. Haug, T. Söderström, O. Cubero, V. Terrazzoni-Daudrix, and C. Ballif, "Plasmonic absorption in textured silver back reflectors of thin film solar cells," J. Appl. Phys. **104**(6), 064509 (2008).
5. A. O. Govorov, J. Lee, and N. A. Kotov, "Theory of plasmon-enhanced Förster energy transfer in optically excited semiconductor and metal nanoparticles," Phys. Rev. B **76**(12), 125308 (2007).
6. S. A. Crooker, J. A. Hollingsworth, S. Tretiak, and V. I. Klimov, "Spectrally resolved dynamics of energy transfer in quantum-dot assemblies: towards engineered energy flows in artificial materials," Phys. Rev. Lett. **89**(18), 186802 (2002).
7. M. Lunz, A. L. Bradley, V. A. Gerard, S. J. Byrne, Y. K. Gun'ko, V. Lesnyak, and N. Gaponik, "Concentration dependence of Förster resonant energy transfer between donor and acceptor nanocrystal quantum dot layers: effect of donor-donor interactions," Phys. Rev. B **83**(11), 115423 (2011).
8. M. Lunz, A. L. Bradley, W.-Y. Chen, V. A. Gerard, S. J. Byrne, Y. K. Gun'ko, V. Lesnyak, and N. Gaponik, "Influence of quantum dot concentration on Förster resonant energy transfer in monodispersed nanocrystal quantum dot monolayers," Phys. Rev. B **81**(20), 205316 (2010).
9. C.-C. Fu, A. Grimes, M. Long, C. G. L. Ferri, B. D. Rich, S. Ghosh, S. Ghosh, L. P. Lee, A. Gopinathan, and M. Khine, "Tunable nanowrinkles on shape memory polymer sheets," Adv. Mater. **21**(44), 4472–4476 (2009).
10. M. I. Stockman, "Femtosecond optical responses of disordered clusters, composites, and rough surfaces: 'the ninth wave' effect," Phys. Rev. Lett. **84**(5), 1011–1014 (2000).
11. Z. Fang, S. Huang, Y. Lu, A. Pan, F. Lin, and X. Zhu, "Color-changeable properties of plasmonic waveguides based on Se-doped CdS nanoribbons," Phys. Rev. B **82**(8), 085403 (2010).
12. H. Du, C. Chen, R. Krishnan, T. D. Krauss, J. M. Harbold, F. W. Wise, M. G. Thomas, and J. Silcox, "Optical properties of colloidal PbSe nanocrystals," Nano Lett. **2**(11), 1321–1324 (2002).
13. A. P. Alivisatos, A. L. Harris, N. J. Levinos, M. L. Steigerwald, and L. E. Brus, "Electronic states of semiconductor clusters: Homogeneous and inhomogeneous broadening of the optical spectrum," J. Chem. Phys. **89**(7), 4001–4011 (1988).
14. H. Zhao, M. Chaker, and D. Ma, "Self-selective recovery of photoluminescence in amphiphilic polymer encapsulated PbS quantum dots," Phys. Chem. Chem. Phys. **12**(44), 14754–14761 (2010).

#179023 - $15.00 USD Received 31 Oct 2012; revised 14 Jan 2013; accepted 16 Jan 2013; published 6 Feb 2013

15. G. V. Shcherbatyuk, R. H. Inman, and S. Ghosh, "Anomalous photo-induced spectral changes in CdSe/ZnS quantum dots," J. Appl. Phys. **110**(5), 053518 (2011).
16. C. R. Kagan, C. B. Murray, M. Nirmal, and M. G. Bawendi, "Electronic energy transfer in CdSe quantum dot solids," Phys. Rev. Lett. **76**(9), 1517–1520 (1996).
17. T. Pons, I. L. Medintz, K. E. Sapsford, S. Higashiya, A. F. Grimes, D. S. English, and H. Mattoussi, "On the quenching of semiconductor quantum dot photoluminescence by proximal gold nanoparticles," Nano Lett. **7**(10), 3157–3164 (2007).
18. H. Szmacinski, K. Ray, and J. R. Lakowicz, "Effect of plasmonic nanostructures and nanofilms on fluorescence resonance energy transfer," J. Biophotonics **2**(4), 243–252 (2009).
19. G. V. Shcherbatyuk, R. H. Inman, C. Wang, R. Winston, and S. Ghosh, "Viability of using near infra-red PbS quantum dots as active materials in luminescent solar concentrators," Appl. Phys. Lett. **96**(19), 191901 (2010).
20. V. Sholin, J. D. Olson, and S. A. Carter, "Semiconducting polymers and quantum dots in luminescent solar concentrators for solar energy harvesting," J. Appl. Phys. **101**(12), 123114 (2007).

1. Introduction

The effect of plasmons on the spectral properties of emitters, both organic and inorganic, has been exploited in biological applications for many years [1]. When there is sufficient spectral overlap between the plasmonic resonance and the absorption band of the emitter, the latter's emission intensity may be enhanced many-fold, a property known as metal enhanced fluorescence (MEF) [2]. More recently, the field of plasmonics has overlapped with other research areas. Plasmons have formed the basis of the design of nano-scale, sub-wavelength components and controls in novel opto-electronic devices [3], and have been incorporated in thin-film photovoltaic modules [4] to allow greater broadband solar absorption for increased efficiency. These applications are based on the direct interactions between the plasmonic fields of metallic films or nanoparticles, and the proximally deposited fluorescent materials like dyes or semiconducting quantum dots (QDs). An indirect extension of this first-order effect is when the plasmons enhance the energy transfer (ET) process between two emitters [5]. The typical mechanism used to describe this ET is known as Forster resonance energy transfer (FRET) [6], a dipolar interaction during which a 'donor' (*D*) non-radiatively transfers its energy to an 'acceptor' (*A*). FRET is strongly distance dependent, falling off as $\sim 1/r^6$ where r is the *D*-*A* separation. However, the strong electric fields of plasmons allow FRET to occur between distant, otherwise non-interacting *D*-*A* pairs, effectively enhancing the spatial range. FRET can also take place within an ensemble of monodispersed QDs [7,8], where the small but inherent size inhomogeneity results in the QD core diameters having a 2-5% variation.

Here, we investigate the extent and efficiency of plasmon-enhanced intra-ensemble FRET between monodispersed QDs when they are deposited onto a wrinkled metallic thin film. We study the typical signatures of intra-ensemble FRET, which include increased recombination rates on the higher energy side of the inhomogenously broadened spectrum, and an accompanied over-all red-shift of the emission. We compare our results with those obtained from control substrates showing weak or no plasmonic modes and conclude that our wrinkled substrates strongly enhanced FRET and increased emission intensities, even in the limit of moderate to low QD deposition concentration, properties that may be useful in QD-based energy harvesting devices.

2. Samples and experimental set-up

In keeping with the idea of possible incorporation of our plasmonic substrates in photovoltaic devices where expense is a critical factor, in place of fabrication-intensive metallic nanoparticles, we use a high throughput, low-cost technique to design metallic nanostructured thin films developed by Fu, et. al [9]. Our substrates are fabricated by sputter-coating a 30 nm thin film of an alloy of gold and palladium (AuPd) on a pre-stressed polydimethylsiloxane **(**PDMS) sheet. This composite is then heat processed following the procedure outlined in ref [9]. Due to the differential thermal expansion of the metallic and non-metallic layers, this results in the former buckling to generate a wrinkled surface. Figure 1(a) is a scanning electron microscopy (SEM) image showing the wrinkles on a typical substrate produced by

#179023 - $15.00 USD Received 31 Oct 2012; revised 14 Jan 2013; accepted 16 Jan 2013; published 6 Feb 2013

this method. Onto these we deposit varying concentrations of CdSe/ZnS core-shell QDs (core diameters ranging from 1.9 – 5.6 nm, Evident Technologies) by spin-coating at 1000 rpm for 10 seconds. For control samples, we deposit CdSe/ZnS QDs on plain glass slides and on 30 nm, flat AuPd films; we also use near infra-red (NIR) PbS QDs as part of the control where the QD sizes are comparable but with greatly varying spectral emission.. For our spectroscopic absorption measurements we use a UV-VIS spectrophotometer (Perkin Elmer). Our photoluminescence (PL) measurements are done using a custom-built scanning confocal microscope with a diffraction-limited optical resolution of ~500 nm which allows us to generate spatially-resolved PL maps. Our excitation sources include a continuous wave diode laser for static PL and an ultrafast Ti:sapphire with a pulse width of 150 fs and a repetition rate of 76 MHz for time-resolved PL measurements. Both lasers are tuned to 405 nm. The QD PL is analyzed by an Acton 2300i spectrometer, which disperses the signal onto a thermo-electrically cooled CCD. For the time-resolved studies we use a time-correlated single photon counting (TCSPC) device (PicoHarp) with a temporal resolution of 4 ps.

3. Results and discussions

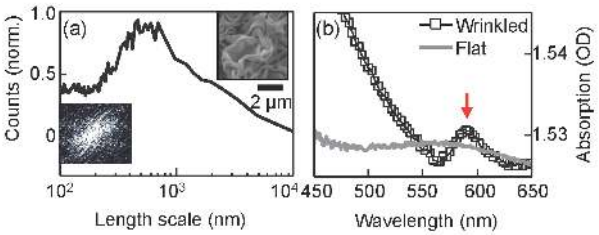

Fig. 1. (a) (inset, top) SEM image of a wrinkled 30 nm AuPd film. (inset, bottom) 2D FFT of SEM image (main) Distribution of length scales of wrinkles derived from 2D FFT of SEM image. (b) Absorption spectra comparing wrinkled and flat metallic surfaces. Arrow shows the plasmon absorption peak of the wrinkled sample.

Our prior work [9] has demonstrated that the wrinkles in Fig. 1(a) have thicknesses that span several hundreds of nanometers. To get a more quantitative estimate, we perform two-dimensional fast Fourier transform (2D FFT) of the SEM image in Fig. 1(a) (inset, top). We observe a diffuse and isotropic FFT pattern in *k*-space, shown in Fig. 1(a) (inset, bottom), which indicates a lack of preferential directionality. Data extracted from the FFT in Fig. 1(a) demonstrates that the wrinkle thickness on this particular substrate vary from 200 nm –1 μm with a mean of 500 nm. This spatial scale, coupled with the randomness in topography and directionality, allows the substrates to exhibit plasmonic functionalities different from the surface plasmon resonances usually observed in continuous metal films. Instead, the resemble localized surface plasmons (LSP) resonances, similar to those observed in metallic nanoparticles [10]. Absorption spectra of the flat AuPd control film in Fig. 1(b) shows a broad absorption peak centered at 550 nm, typical of continuous films. In comparison, the wrinkled film shows a sharp peak at 580 nm, a signature more like an LSP resonance.

#179023 - $15.00 USD Received 31 Oct 2012; revised 14 Jan 2013; accepted 16 Jan 2013; published 6 Feb 2013

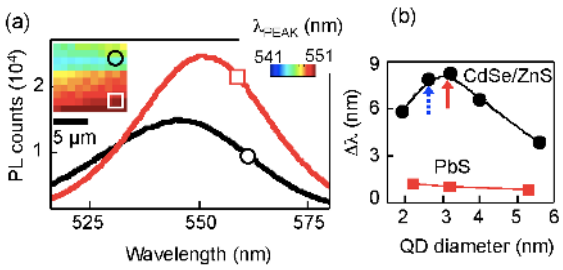

Fig. 2. (a, inset) Scanning PL image of QD (λ_S = 544 nm) peak emission wavelength (λ_{PEAK}) deposited on wrinkled surface. (main) QD spectra from two regions of the scanned surface. Symbols correspond to area on surface in inset. (b) spectral red-shifts ($\Delta\lambda$) observed in CdSe/ZnS and PbS QDs deposited on wrinkled films plotted as functions of QD diameter. Dashed and solid arrows indicate sizes of QDs with λ_S of 544, and 586 nm, respectively.

The first sample of QDs studied on the wrinkled film have core diameters ~2.4 nm, with a peak emission wavelength in solution (denoted λ_S) of 544 nm. A scanning PL map of the peak emission wavelength (λ_{PEAK}) from a 10 × 10 μm^2 area of QD coated film is shown in the inset of Fig. 2(a). λ_{PEAK} is red-shifted over a substantial portion of the scanned area. Comparing the spectra from an unshifted (circle marker) and red-shifted (square marker) regions of the scan in Fig. 2(a), we additionally observe an emission intensity enhancement accompanying the spectral shift. This can be attributed to MEF, and given the non-uniformity of the wrinkles, the observed spatial variation in the extent of MEF is unsurprising. We repeat these measurements with CdSe/ZnS QDs of sizes varying between 1.9 – 5.6 nm in diameter and observe a spectral shift in every sample, although of varying magnitudes. We quantify the maximum red-shift as $\Delta\lambda = \lambda_{PEAK} - \lambda_S$, where λ_S is the solution peak emission. $\Delta\lambda$, plotted in Fig. 2(b) (solid circles) as a function of QD size, varies non-monotonically with it and has a maximum for those QDs, indicated by arrows [Fig. 2(b)], whose emission spectra has most overlap with the plasmonic resonance of the wrinkled films, typically centered at 580 nm [Fig. 1(b)].

There are two possible mechanisms that may give rise to spectral red-shifts in an ensemble of QDs. On a microscopic level, plasmons are oscillating electric fields, and can induce Stark shifts in QDs [11]. This shows up as red-shifts, but is strongly dependent on the power of the excitation source where the red-shift gets larger with increasing power,, We do not observe any such power dependence. Further, there is no reason for an optical Stark shift to vary with QD size and produce the trend we observe in Fig. 2(b). The other option is increased FRET between the QDs, when the smaller QDs (which emit at shorter wavelengths) transfer energy to the larger dots, causing the peak of the overall emission to shift towards a longer wavelength [8]. The question that needs to be asked is what could be the cause of enhanced FRET on the wrinkled films? One possibility is that the topography of the wrinkles allows close-packing of the deposited QDs, decreasing the inter-dot separation and increasing their dipolar coupling. However, this purely geometric effect should again not have the size dependence of Fig. 2(b). The QD diameters we study are between 1.9 – 5.6 nm. This size variation is negligible when compared to the hundreds of nanometers length scale of the wrinkles. QDs of all sizes should pack equally efficiently on the wrinkled surfaces, and show equivalent amount of FRET, which they appear to not. As a further check, we deposit PbS QDs at the same concentration on the wrinkled films. The diameter of these dots are comparable to the CdSe/ZnS QDs, as shown in Fig. 2(b), but their emission is in the near infra-red region (> 850 nm), implying no spectral overlap with the plasmon absorption of the films. PbS QDs demonstrate large intra-ensemble FRET [12] if close-packed, but we do not observe comparable red-shifts in Fig. 2(b) for PbS QDs, which leads us to conclude that it is not topography-induced close-packing, that is causing increased FRET.

#179023 - $15.00 USD Received 31 Oct 2012; revised 14 Jan 2013; accepted 16 Jan 2013; published 6 Feb 2013

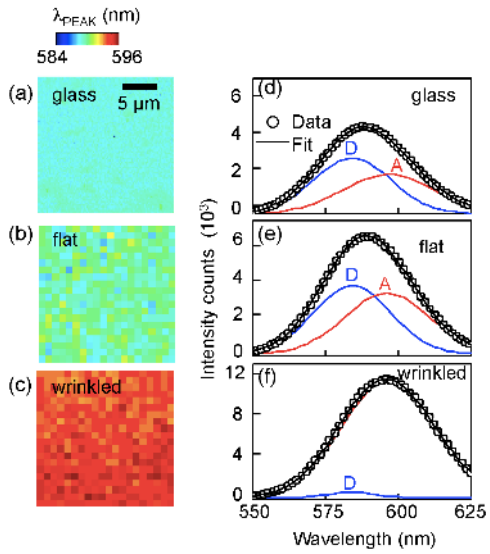

Fig. 3. Scanning PL images of λ_{PEAK} of QDs (λ_S = 586 nm) spin coated on to (a) glass, (b) flat metal film, and (c) wrinkled metal film. Spectral emission from (d) glass, (e) flat, and (f) wrinkled surface. Open circles represent emission data. Lines are Gaussian fits (see text for details) with the short and long wavelength curves labelled D and A, respectively

FRET occurs between QDs as a result of the coupling of their electric dipole moments, where spatial proximity is the key determinant. It has been previously reported that plasmons can mediate this dipolar interaction, extending the range over which FRET may occur [5]. In the following, we perform further measurements to verify that we can attribute our observations to plasmonic enhancement of FRET. We begin by repeating our measurements with QDs that have λ_S = 586 nm, indicated by the solid arrow in Fig. 2(b), since they show the largest red-shift. A QD solution of 0.3 μM is spin-coated on a glass slide, a flat 30 nm film and a wrinkled 30 nm film. Scanning PL maps of λ_{PEAK} are shown in Figs. 3(a)–3(c). On the glass slide in Fig. 3(a), the emission is uniform, indicating good QD coverage, and there is an average red-shift ~1 nm. A representative spectrum is shown in Fig. 3(d). Any typical ensemble of chemically synthesized QDs has a finite size distribution, and the resultant emission spectrum is inhomogenously broadened [13]. This continuous variation in QD size makes it impossible to clearly delineate donors from acceptors for the specific analysis of energy transfer. However, we may model the spectrum in Fig. 3(d) as a cumulative of two individual Gaussian distributions, representing a donor ('*D*', shorter wavelength) subset and an acceptor ('*A*', longer wavelength) subset, following prior observations of such populations [12–15]. On the glass slide the donor subset has a slightly greater weight, indicating very small amount of FRET in the ensemble, in agreement with Fig. 3(a). The flat metal film in Fig. 3(b) shows isolated regions of small red-shifts and a spectrum in Fig. 3(e) shows increased emission intensity as well. Using the fits, we notice a more equitable distribution between the two subsets. The wrinkled film in Fig. 3(c) shows large and relatively uniform red-shift over the scanned area. A spectrum in Fig. 3(f) shows that the emission is now almost entirely a contribution of the longer wavelength acceptor subset, with the donor subset having negligible spectral weight. The integrated emission intensity is greater by a factor of 3 compared to the emission from the glass slide, and twice as large as that from the flat film. Comparing the results from the flat and wrinkled films we can deduce that both intensity enhancement and spectral red-shift occur to varying degrees on both, but they are much more emphatic on the wrinkled substrate, which is in agreement with their relative plasmonic resonances [Fig. 1(b)].

#179023 - $15.00 USD Received 31 Oct 2012; revised 14 Jan 2013; accepted 16 Jan 2013; published 6 Feb 2013

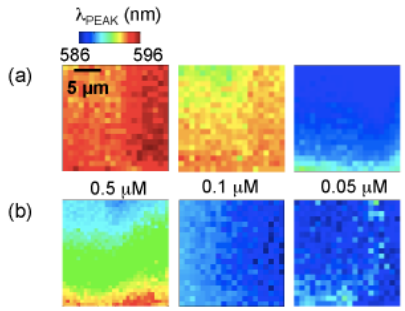

Fig. 4. Scanning PL images of λ_{PEAK} of QDs (λ_S = 586 nm) deposited on (a) wrinkled metal film and (b) glass, at 3 different QD concentrations.

To further demonstrate the efficacy of our wrinkled substrates in enhancing FRET in QDs, we vary the QD solution concentration and plot the spatially-resolved peak wavelength maps of the resultant samples on both wrinkled metallic and glass substrates in Figs. 4(a) and 4(b), respectively. Transmission electron microscopy on the glass substrates gives us an estimate of the inter-dot spacing in these samples. For the lowest concentration of 0.05 μM, the average separation between QDs is on the order of 30-40 nm. Given this is almost ten times the FRET radius [7], we unsurprisingly do not observe red-shift on either substrate. At 0.1 μM, the inter-QD separation decreases to an average of 20-25 nm, which is still substantially large compared to distances over which FRET is efficient. As a result, the QDs on glass demonstrate no red-shifting. In contrast, we do observe between 3 – 5 nm of spectral shift between QDs on the metal film, clearly indicating FRET in enhanced no these substrates. On the most concentrated sample, the QDs are separated by 10 – 15 nm and FRET can be observed both on glass and the metallic film, though it is more uniform and has a greater impact on the latter.

Aside from static spectral signatures, introduction of any coupling between QDs and another entity, such as other QDs, plasmons, cavity modes etc., always lead to changes in the exciton recombination rates [16]. Time-resolved PL is therefore a very useful tool that allows us to observe changes in exciton dynamics, and the information gleaned from it sheds considerable light on the nature of the mechanism behind the changes. In Fig. 5(a) we plot the spectrally-integrated dynamic PL for all 3 samples examined in Fig. 3. In solution, the QD recombination process can be described by an exponential decay $I(t) = I_0 \exp(-t/\tau_S)$ characterized by a single lifetime τ_S = 13 ns for these QDs. Emission from the glass slide is still a single exponential decay, and the lifetime τ_G = 11 ± 0.3 ns. On the flat film we see the emergence of a second lifetime, and the recombination process is now better described as: $I(t) = I_1 \exp(-t/\tau_1) + I_2 \exp(-t/\tau_2)$. The shorter time scale τ_1 is 2 ± 0.2 ns, but the longer lifetime, τ_2 = 10 ± 0.4 ns, is almost unchanged from the glass sample given the margin of error. The wrinkled film has a recombination curve similar to the flat film, but with comparable τ_1 (1.6 ± 0.07 ns) and shorter τ_2 (8 ± 0.4 ns). We measure the QD recombination times for a total of ten samples, and the data shown in Fig. 5(b) allow us to draw two conclusions: first, they indicate that the fast decay τ_1 is independent of the texture of the metal films, and as it is not observed on the glass slide, we conclude that this corresponds to fast of PL quenching [17], commonly observed on metallic surfaces; second, it confirms that the QDs on the wrinkled films consistently have higher recombination rates. In addition, the data also allows us to calculate the wavelength averaged FRET efficiency $\varepsilon = 1 - (\tau_{substrate}/\tau_S)$ [18], where $\tau_{substrate}$ is the intensity-weighted average lifetime of each substrate [7]. For the

#179023 - $15.00 USD Received 31 Oct 2012; revised 14 Jan 2013; accepted 16 Jan 2013; published 6 Feb 2013

glass slide ε is typically 15%, but increases to 20 - 23% in the flat films and is between 39 – 42% in the wrinkled films, a factor of about 2.5 more than on glass. A consequence of this higher energy transfer efficiency is shown in Fig. 5(a) (inset). As the QD PL moves to longer wavelengths, the spectral overlap between the emission and absorption bands decreases. By comparing the normalized absorption and emission spectra, we calculate that for the wrinkled film the overlap is almost 30% less than in the case of the glass substrate.

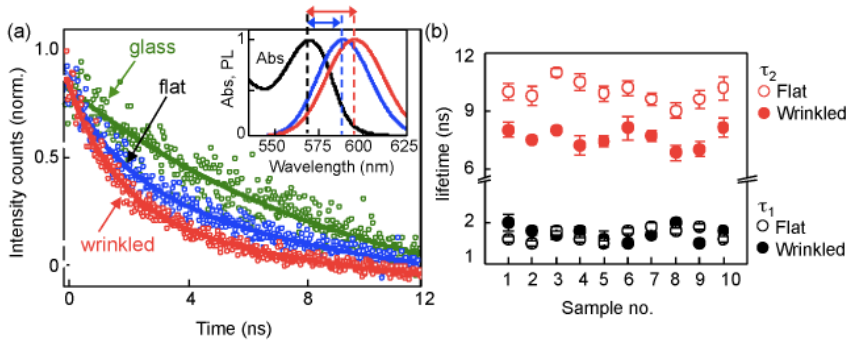

Fig. 5. (a) Time-resolved PL comparing the QD recombination on glass, flat metal and wrinkled metal surfaces. Lines are exponential fits. (inset) Normalized PL spectra of QDs deposited on glass (blue) and wrinkled (red) surfaces alongside the QD absorption (black) curve. The dashed lines indicate the spectral positions of the peaks, and the double headed arrows show the effective Stoke's shifts for QDs on glass (blue) and wrinkled metal (red) surfaces. (b) The short (τ_1) and long (τ_2) QD recombination times for ten different flat (open circles) and wrinkled (filled circles) samples.

4. Conclusions

The spectral red-shift that results as a consequence of intra-ensemble FRET, in turn decreasing the overlap between emission and absorption bands, reducing the occurrence of 'self-absorption'. Self-absorption is a phenomenon where a QD sample re-absorbs its emitted photons and is a critical limiting factor in QD-based luminescent energy harvesting devices [19,20]. The plasmon-mediated effects observed here include a 30% reduction of spectral overlap between absorption and emission bands of the QD spectra, accompanied by three-fold higher emission intensities, both highly desirable properties for application in photovoltaic devices, which will lower self-absorption and increase device efficiency. More importantly, our use of easily fabricated, inexpensive and eminently scalable nano-wrinkled metal films as the plasmonic substrates makes our findings particularly attractive.

Acknowledgments

We would like to acknowledge support from NSF grant EF-1038697, DMR-0821771, DMR-1056860, James S. McDonnell Foundation Award and NIH New Innovator 1DP2OD007283.